IOPscience iopscience.iop.org

Home Search Collections Journals About Contact us My IOPscience

Magnetic subunits within a single molecule–surface hybrid

This content has been downloaded from IOPscience. Please scroll down to see the full text.

2017 New J. Phys. 19 053016

(http://iopscience.iop.org/1367-2630/19/5/053016)

View the table of contents for this issue, or go to the journal homepage for more

Download details:

IP Address: 152.3.194.117
This content was downloaded on 06/07/2017 at 21:16

Please note that terms and conditions apply.

You may also be interested in:

First-principles insights into the electronic and magnetic structure of hybrid organic-metal interfaces
Predrag Lazi, Vasile Caciuc, Nicolae Atodiresei et al.

Interface-induced chiral domain walls, spin spirals and skyrmions revealed by spin-polarized scanning tunneling microscopy
Kirsten von Bergmann, André Kubetzka, Oswald Pietzsch et al.

Spin-polarized scanning tunnelling microscopy
M Bode

Controlling the magnetism of adsorbed metal–organic molecules
Wolfgang Kuch and Matthias Bernien

Local tunnel magnetoresistance of an iron intercalated graphene-based heterostructure
R Decker, M Bazarnik, N Atodiresei et al.

Atomically crafted spin lattices as model systems for quantum magnetism
A Spinelli, M P Rebergen and and A F Otte

Change of cobalt magnetic anisotropy and spin polarization with alkanethiolates self-assembled monolayers
Paolo Campiglio, Romain Breitwieser, Vincent Repain et al.

Complex magnetism of the Fe monolayer on Ir(111)
Kirsten von Bergmann, Stefan Heinze, Matthias Bode et al.

New Journal of Physics
The open access journal at the forefront of physics

Deutsche Physikalische Gesellschaft DPG
IOP Institute of Physics

Published in partnership with: Deutsche Physikalische Gesellschaft and the Institute of Physics

OPEN ACCESS

RECEIVED
31 January 2017

REVISED
23 March 2017

ACCEPTED FOR PUBLICATION
24 April 2017

PUBLISHED
17 May 2017

Original content from this work may be used under the terms of the Creative Commons Attribution 3.0 licence.

Any further distribution of this work must maintain attribution to the author(s) and the title of the work, journal citation and DOI.

PAPER

Magnetic subunits within a single molecule–surface hybrid

Volkmar Heß[1,2,3], Rico Friedrich[3,4], Frank Matthes[1,3], Vasile Caciuc[3,4], Nicolae Atodiresei[3,4,5], Daniel E Bürgler[1,3,5], Stefan Blügel[3,4] and Claus M Schneider[1,3]

[1] Peter Grünberg Institut (PGI-6), Forschungszentrum Jülich, D-52425 Jülich, Germany
[2] Institut für Anorganische Chemie, RWTH Aachen University, D-52074 Aachen, Germany
[3] Jülich-Aachen Research Alliance, Fundamentals of Future Information Technology (JARA-FIT), D-52425 Jülich, Germany
[4] Peter Grünberg Institut (PGI-1) and Institute for Advanced Simulation (IAS-1), Forschungszentrum Jülich, D-52425 Jülich, Germany
[5] Authors to whom any correspondence should be addressed.

E-mail: n.atodiresei@fz-juelich.de **and** d.buergler@fz-juelich.de

Keywords: magnetic molecule–surface hybrids, molecular spintronics, spin-polarized scanning tunneling microscopy

Supplementary material for this article is available online

Abstract

Magnetic molecule–surface hybrids are ideal building blocks for molecular spintronic devices due to their appealing tailorable magnetic properties and nanoscale size. So far, assemblies of interacting molecular-surface hybrids needed for spintronic functionality were generated by depositing aromatic molecules onto transition-metal surfaces, resulting in a random arrangement of hybrid magnets due to the inherent and strong hybridization. Here, we demonstrate the formation of multiple intramolecular subunits within a single molecule–surface hybrid by means of spin-polarized scanning tunneling microscopy experiments and *ab initio* density functional theory calculations. This novel effect is realized by depositing a polycyclic aromatic molecule on a magnetic surface. A highly asymmetric chiral adsorption position induces different structural, electronic, and magnetic properties in each aromatic ring of the molecule. In particular, the induced molecular spin polarization near the Fermi energy varies among the rings due to site- and spin-dependent molecule–surface hybridization. Our results showcase a possible organic chemistry route of tailoring geometrically well-defined assemblies of magnetically distinguishable subunits in molecule–surface hybrids.

1. Introduction

In the past few years molecular spintronics [1] research has witnessed a fast developing interest in the investigation and functionalization of organic–ferromagnetic interfaces [2–16]. Major achievements in the field include the detection of the inversion of the spin-polarization above single molecules deposited on magnetic surfaces [7, 8, 12, 16], the measurement of interface magnetoresistance due to the formation of a hybrid interface magnetic layer [11], and the time-resolved occupation analysis of hybrid interface states acting as spin-dependent electron traps [10].

The adsorption of a nonmagnetic π-conjugated organic molecule on a ferromagnetic surface can lead to the magnetic hardening effect and thus the creation of a so-called magnetic molecule–surface hybrid [1, 7, 8, 15] with a stable magnetization direction and an enhanced coercive field as compared to the clean surface [17]. The magnetic moment, anisotropy, and coercive field of these hybrids sensitively depend on the spin-dependent hybridization of molecular π-orbitals with *d*-orbitals of the substrate [7, 13, 14], which is governed by the local geometry and chemical bond formation. Recently, the long-range magnetic coupling of molecule–surface hybrids embedded in a nanoskyrmion lattice was demonstrated [13] offering a molecular analogy to the atom-by-atom spin-based logic devices realized by single atomic chains connected to ferromagnetic leads [18]. So far, the possible presence of magnetically distinguishable subunits in a single magnetic molecule–surface hybrid has not been considered. Theoretical work dealing with the chemisorption of a variety of carbon-based molecules [17, 19] showed that the spin-dependent π–*d* hybridization between molecules and ferromagnetic substrates enhances the exchange coupling among the involved substrate atoms. Here, we demonstrate that in more

© 2017 IOP Publishing Ltd and Deutsche Physikalische Gesellschaft

complex polyaromatic molecules this effect occurs for each aromatic ring and can indeed induce magnetically distinguishable subunits. To this end, we study nanoscale organic–ferromagnetic hybrid systems formed by depositing polycyclic 2,4,6-triphenyl-1,3,5-triazine (TPT) molecules comprising in total four phenyl and triazine-like rings on two monolayers (ML) Fe on W(110). Our combined spin-polarized scanning tunneling microscopy (SP-STM) and density functional theory (DFT) investigation uncovers significant ring-to-ring differences in local density of states (LDOS) and spin polarization as well as magnetic couplings arising from a highly asymmetric adsorption geometry. The advantage of such a molecular approach is the possibility to tailor the geometry of the assembly of hybrid magnetic units and their magnetic properties by means of synthetic organic chemistry.

2. Methods

2.1. Experiment

Samples were prepared under ultra-high vacuum (UHV) conditions. The W(110) substrate was cleaned according to the procedure described in [20]. Iron was evaporated at a rate of 0.6 ML min^{-1} for a total coverage of 1.5 ML. To achieve smooth surfaces samples were annealed at 500 K for 8 min. TPT was obtained from Sigma-Aldrich with a purity of 98% and was sublimed after thoroughly degassing at 450 K from a Knudsen cell with a rate of 0.5 ML min^{-1}. During the TPT deposition the substrate was cooled to 170 K to reduce the molecule mobility on the surface. Afterwards the sample was transferred into the STM and cooled to 5 K. SP-STM images were obtained with Cr-coated (10 ML) W-tips. dI/dV spectra are recorded by modulating the bias voltage (4.111 kHz, 30 mV_{rms}) and using lock-in detection. All displayed spectra are taken during a single bias voltage ramp. For each voltage step, the lock-in amplifier is allowed to stabilize for 10 ms, before the dI/dV signal is averaged during 40 ms. The positioning accuracy and the reproducibility of the relevant features is ensured by repeating the measurements several times.

2.2. Theory

The spin-polarized electronic structure calculations were carried out in the framework of DFT [21, 22] using the VASP program [23–25]. In addition, projector augmented-wave datasets [26] as constructed for the exchange-correlation functional of Perdew, Burke, and Ernzerhof [27] were employed. Throughout all calculations a plane wave cutoff energy of 500 eV was used. All structures were relaxed until the forces were smaller than 10 meV $Å^{-1}$. Due to the large size of the supercell (22.4 Å × 22.2 Å × 33.1 Å) used in the calculations, the Brillouin zone was sampled only at the Γ-point. The unit cell consisted of two Fe layers and five W layers [2 ML Fe/W(110)] each represented by a 5 × 7 in-plane surface unit cell containing 70 Fe or W atoms. The TPT molecule was adsorbed on top of the Fe layers. The vertical (vacuum) spacing between two slabs was about 18 Å, and the lateral distance between molecules in neighboring unit cells was at least 10 Å. During the geometry optimization the upper two W layers, the two Fe layers, and the atoms in the molecule were allowed to relax.

3. Results

3.1. Adsorption geometry and electronic properties

The flat molecular structure of TPT consists of three peripheral phenyl rings attached to a central triazine-like ring (figures 1(b) and (c)). Hence it consists of two types of aromatic rings, which are chemically and consequently also electronically different. Considering previous reports [13, 17], it can be expected that upon adsorption of the molecule on a magnetic surface (at least) two different magnetic subunits will be formed. Furthermore, the degeneracy among the peripheral phenyl rings can be lifted depending on the symmetry of the substrate lattice and the resulting adsorption geometry.

For this reason we first characterize the deposition of TPT on 2 ML Fe/W(110) by STM. All STM measurements have been performed at 5 K under UHV conditions. Figure 1(a) shows a typical overview STM image with sub-monolayer TPT coverage. The TPT molecule is easily identified by its characteristic shape (figure 1(b)) and is reliably found on defect-free areas. The clearly predominant occurrence of intact and unperturbed TPT molecules indicates a sufficient molecular stability against decomposition during sublimation and surface deposition. The vertical stripes in figure 1(a) are characteristic dislocation lines of the 2 ML Fe/W (110) surface [28].

A closer inspection of the TPT appearance, e.g. in the inset in figure 1(a), reveals differences for the peripheral phenyl rings in brightness, size, and shape. The bottom right phenyl ring (‘1’) in the inset in figure 1(a) appears in the STM images brightest and almost spherical. In comparison, the left (‘2’) and the top right (‘3’) phenyl rings appear smaller and darker. The significance of these differences is shown in figure S3 of the supplementary online material available at stacks.iop.org/NJP/19/053016/mmedia. Since in the gas phase

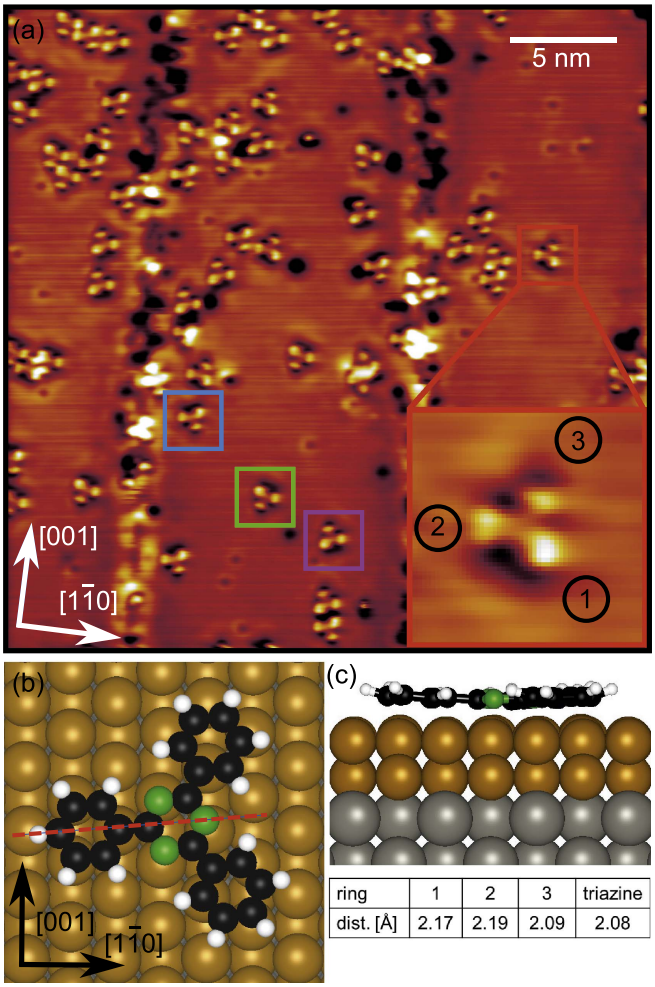

ring	1	2	3	triazine
dist. [Å]	2.17	2.19	2.09	2.08

Figure 1. Adsorption geometry. (a) Overview STM topography image of TPT on 2 ML Fe/W(110) taken at $V_{\mathrm{Bias}} = -100$ mV and $I_{\mathrm{T}} = 1$ nA. Differently colored boxes mark the four observed chiral adsorption orientations. Inset: zoom of an adsorbed TPT molecule (image size 3 × 3 nm^2). (b) Topview and (c) sideview of the relaxed adsorption geometry of TPT on 2 ML Fe/W(110) determined by DFT. The orientation of the molecule is the same as in the inset of (a) (black—carbon, green—nitrogen, white—hydrogen). Adsorption heights in the table are measured from the topmost Fe layer of the bare Fe surface.

geometry all phenyl rings exhibit the same electronic properties, these differences must arise from the interaction with the 2 ML Fe/W(110) surface. STM measurements of TPT with atomic resolution of the substrate lattice (see note 1 in the supplementary online material) reveal a completely asymmetric adsorption geometry, for which each aromatic ring exhibits a different binding to the substrate. Consequently intramolecular differences in LDOS arise among the rings and are detected by STM. A computational investigation of the stability of different adsorption geometries corroborates the experimentally suggested adsorption geometry as having the largest binding energy to the surface (see note 1 in the supplementary online material). The lowest-energy relaxed structure is presented in figures 1(b) and (c). The sideview in figure 1(c) reveals different adsorption heights of the distinct aromatic rings as a manifestation of the asymmetric adsorption geometry. The lowest adsorption height is associated with the central triazine-like ring that is most tightly bound to the surface in agreement with [29]. When adsorbed on the 2 ML Fe/W(110) surface one mirror plane of the TPT molecule (red line in figure 1(b)) is rotated by $\pm 7°$ with respect to the [1 $\bar{1}$0] direction of the substrate, giving rise to a chiral adsorption geometry. All four resulting chiral adsorption orientations are experimentally observed as shown by the molecules marked with different colors in figure 1(a). Adsorption-induced molecular chirality [30, 31] has previously been evidenced by STM observation [32–35]. A more detailed discussion of the chiral adsorption positions is given in note 2 in the supplementary online material.

The LDOS differences between the phenyl rings arising from the asymmetric adsorption position were further investigated by scanning tunneling spectroscopy (STS). Spectra of each aromatic ring as well as a reference spectrum of the substrate are presented in figure 2(a). Tip changes during the experiment were excluded by comparing spectra of the bare substrate before and after the measurements. The characteristic d_{z^2} orbitals for the 2 ML Fe/W(110) at −80 and +700 mV are easily identified [36]. The phenyl rings are numbered with respect to decreasing brightness, i.e. the same way as in the inset of figure 1(a). The molecular spectra do not

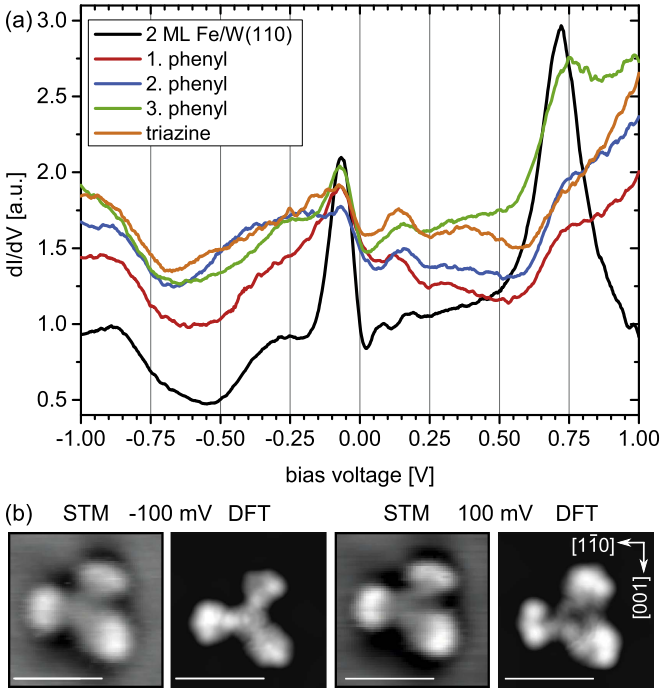

Figure 2. Electronic properties. (a) STS spectra taken above all four aromatic rings of an adsorbed TPT molecule (tip stabilized at $V_{Bias} = -100$ mV and $I_T = 1$ nA). The LDOS differences between the three phenyl rings arise solely from their different binding to the substrate. (b) Comparison of measured STM and simulated DFT topography images at $V_{Bias} = +100$ and -100 mV. All scale bars equal 1 nm.

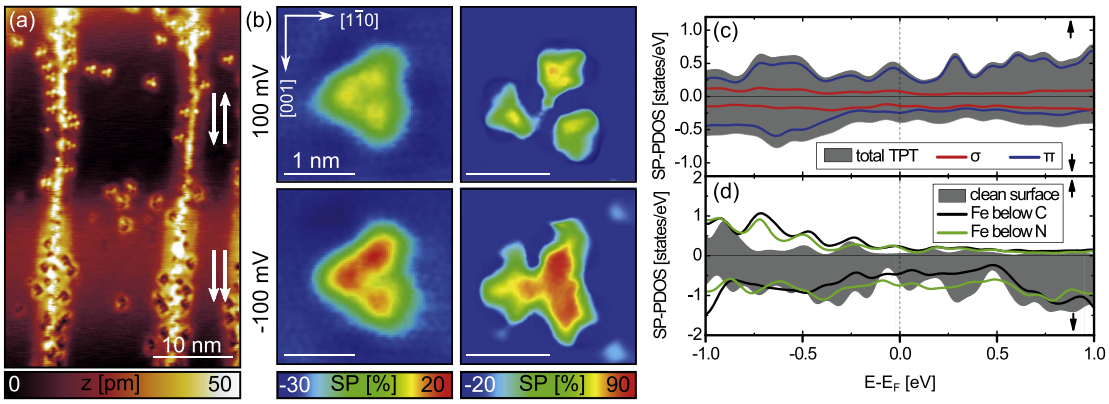

Figure 3. Molecular spin polarization. (a) SP-STM topography overview image with TPT molecules on two opposite magnetic domains (dark/bright) taken at $V_{Bias} = 100$ mV and $I_T = 1$ nA. The white arrows indicate relative alignment of tip and sample magnetizations. (b) Comparison of the measured (first column) and simulated (second column) spin polarization (SP) maps at $V_{Bias} = \pm 100$ mV. All scale bars are 1 nm. (c) Calculated SP-PDOS of TPT on 2 ML Fe on W(110). Blue and red curves represent the π and σ contributions, respectively. (d) SP-PDOS of the bare Fe surface and of Fe atoms located below a C (black) or N (green) atom of the TPT molecule. The spin polarization near the Fermi energy is clearly negative in all three cases.

exhibit sharp peaks, but instead show broad band-like features due to the hybridization with the substrate. This situation is typical for chemisorption and indicates a strong interaction between molecule and surface in agreement with the large calculated adsorption energy of 3.58 eV. Significant peaks in the molecular spectra are found at the same energy as the Fe d_{z^2} orbitals of the bare substrate. The assignment of these peaks to spectral features of the TPT/Fe molecule–surface hybrid system that originate from molecular π states is confirmed in the simulated LDOS presented in figure 3(c). The inequivalent hybridization of the three peripheral phenyl rings with the substrate results in a different shape of the corresponding peaks and induces LDOS differences affecting the whole investigated bias voltage interval of [−1 V, 1 V]. Interestingly, the triazine-like ring exhibits a similar spectrum as the phenyl rings. Aromatic rings with varying number of nitrogen atoms have been shown to exhibit significantly different electronic properties [37]. In the present case the proximity of the aromatic rings and the finite radius of the STM tip appear to reduce these differences.

Figure 2(b) compares experimentally measured topography images taken at ±100 mV with corresponding calculations performed in the Tersoff–Hamann approximation [38]. Differences between the aromatic rings concerning appearance and lateral extent are clearly visible in the STM data at both bias voltages and are nicely reproduced in the simulated images in figure 2(b).

3.2. Magnetic properties

The magnetic properties of the TPT/Fe/W(110) system are investigated by SP-STM using Cr-coated W-tips sensitive to the out-of-plane magnetization direction. An SP-STM overview topography image of the TPT/Fe/W(110) system is shown in figure 3(a). Similar to previous reports on other organic–ferromagnetic interfaces [7], TPT appears in SP-STM topographies significantly different on opposite magnetic domains (dark and bright background in figure 3(a)). On domains where tip and sample magnetization are antiparallel (dark domain), the TPT appears very similar to the spin-integrated case in figure 1(a). In contrast, on domains with parallel tip and sample magnetizations (bright), TPT is imaged as a mostly black spot with a bright halo. These marked differences in appearance indicate a strong spin-dependent hybridization.

Spin polarization maps of the TPT/Fe/W(110) system are analyzed in figure 3(b). The spin polarization maps are calculated according to the procedure described in [7, 39] by subtracting SP-STM topography images of TPT on oppositely magnetized domains. In contrast to previous work [7, 40, 41] we find within a given adsorbed molecule different spin polarization with specific features on aromatic rings (here the phenyl rings) that are otherwise chemically identical in the gas phase. For the theoretical data the height difference represents the spin polarization of the sample, whereas for the experimental data it is approximately proportional to the effective polarization of the tip-sample tunneling junction (see note 3 in the supplementary online material). The spin polarization of the tip that is not entering the calculations can be considered constant during a given measurement and solely reduces the experimentally measured effective polarization. Experimental and simulated raw images used for the calculation of the spin polarization maps are presented in figure S4 in the supplementary online material. The comparison of the spin polarization maps in figure 3(b) again indicates a good qualitative agreement between experiment and theory[6]. One important point is that for the bare Fe surface close to the Fermi level minority (spin-down) states dominate. Therefore, the spin polarization P of the bare Fe surface close to the Fermi energy

$$P = \frac{n^{\uparrow} - n^{\downarrow}}{n^{\uparrow} + n^{\downarrow}} \tag{1}$$

is negative, where $n^{\uparrow}$ and $n^{\downarrow}$ are the charge densities for spin-up and spin-down in a given energy interval. Remarkably, the spin polarization at both bias voltages is clearly positive above the molecule, i.e. it is inverted in agreement with the theoretically predicted and experimentally observed general $p_z - d$ hybridization-induced inversion of the spin polarization above non-magnetic organic molecules chemisorbed on magnetic substrates [7, 16]. The inversion of the spin polarization above the molecule extends over a large energy range around the Fermi energy as can be clearly seen in the calculated spin polarized density of states (SP-PDOS) on the site of the molecule depicted in figure 3(c). STM accesses practically solely the π states (blue line) above the molecule since the σ states are predominantly localized in the molecular plane and thus decay more rapidly into the vacuum region. On the other hand, the SP-PDOS of the surface Fe atoms even below the molecule in figure 3(d) clearly indicates a negative spin polarization P hence pointing to the molecular origin of the observed inversion. In addition, the simulated images in figure 3(b) correctly reproduce the smaller degree of positive spin polarization above the TPT molecule at +100 mV as compared to −100 mV, where above two molecular rings very strong positive spin polarization is detected. However, the relative degree of the spin polarization among the lobes is slightly different between experiment and theory. This minor difference can be assigned to the electronic structure of the tip, which is contributing to the measurements, but is not included in the simulations according to the Tersoff–Hamann approximation. Most importantly, in both the experimental and the theoretical results a pronounced difference in the spin polarization among the lobes is found, which is particularly obvious at −100 mV. This means that the structural asymmetry outlined above carries over not only to the electronic (figure 2(a)) but also to the magnetic properties of the system. Hence, the magnetic inequivalence of the four subunits related to the four aromatic rings of TPT is established.

The spin-dependent hybridization at organic–ferromagnetic interfaces not only induces spin polarization in the chemisorbed molecules, but also modifies the magnetic properties of the involved substrate atoms. More precisely, when analyzing the magnetic moments and molecule–surface distances within the relaxed structure obtained from DFT for the TPT-2 ML Fe/W(110) hybrid system we found that the interaction of TPT with the surface is essentially confined to the thirteen first layer Fe atoms it is directly bound to (green and black marked atoms in figure 4(a)) in agreement with previous findings in [17, 19, 29, 42]. Specifically, for these 13 Fe surface

[6] When comparing experimental (SP-)STM images with simulated images, one has to be aware that the STM tip is an integral part of the quantum-mechanical system describing the tunneling junction of the STM experiment, which is not accounted for in the simulations.

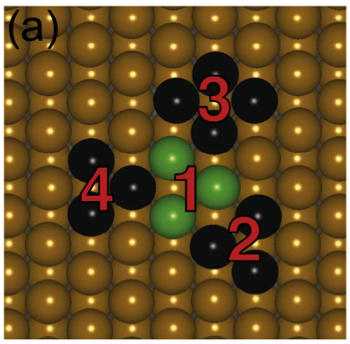

(b)

unit	m_{unit} (μ_B)	J_{unit} (meV)
1Fe-cs	2.9	403
1	8.1	811
2	7.7	746
3	10.4	872
4	7.6	765

Figure 4. Intramolecular magnetic subunits. (a) Assignment of the 13 Fe atoms of the TPT on the 2 ML Fe/W(110) system involved in the hybridization to the hybrid magnetic subunits 1–4 below the four different rings of the TPT molecule. (b) Calculated magnetic moment m_{unit} and exchange coupling constant J_{unit} of each intramolecular magnetic subunit compared to the values for a single surface Fe atom of the bare surface (1Fe-cs). The moment of subunit 3 is about 2.5 μ_B larger than the others since it comprises four instead of three Fe surface atoms.

atoms the distance to C or N atoms of the molecule is shorter than 2.5 Å, whereas all other surface atoms are at larger distances. In addition, the magnetic moments of these 13 Fe atoms are considerably reduced by 0.1–0.5 μ_B compared to the bare surface value of 2.9 μ_B, whereas all other Fe moments are equal to the clean surface value (see table S2 of note 4 in the supplementary online material). Furthermore, experiments [13, 43] as well as DFT calculations [17, 19, 42] have unambiguously shown that carbon-based adsorbates such as organic molecules and graphene lead to an in-plane magnetic hardening effect, i.e. they enhance the exchange coupling between the first layer magnetic surface atoms directly bound to them. Even more importantly, in [17] it was demonstrated that due to this effect the chemisorbed benzene-like ring of paracyclophane gives locally rise to the formation of a strongly exchange coupled hybrid molecule–surface magnetic unit. Based on these grounds and the magnetic non-equivalence of all aromatic rings of TPT on Fe/W(110) outlined in figure 3(b) the chemisorbed TPT molecule can be considered to give rise to four molecule-induced magnetic subunits, each consisting of an aromatic ring and the Fe atoms directly bound to it. The assignment of the Fe surface atoms to different magnetic subunits labeled 1–4 is shown in figure 4(a).

We evaluated the magnetic exchange coupling constants between these subunits and of each subunit to its clean Fe environment by generalizing the procedure used in [17, 19, 29]. Each magnetic subunit is coupled to a specific clean surface unit that consists of the respective unperturbed nearest-neighbor Fe atoms in the first and second Fe layers. The exchange interaction is modeled by a nearest-neighbor Heisenberg Hamiltonian:

$$H_{\text{units}}^{\text{spin}} = -\sum_{\langle i>j\rangle} J_{ij} m_i m_j, \tag{2}$$

where m_i and m_j stand for the values of the magnetic moments of nearest-neighbor units i and j, respectively. Accordingly, the energy difference between ferromagnetic (FM) and antiferromagnetic (AFM) alignment of specific magnetic subunits can be expressed as:

$$E_{\text{FM}} - E_{\text{AFM}} = -2\sum_{\langle i>j\rangle} J_{ij} m_i m_j. \tag{3}$$

By taking into account a suitably chosen set of antiferromagnetic configurations, where the moments of selected magnetic subunits are flipped, the coupling constants between the subunits can be obtained from the resulting system of coupled equations (see note 4 in the supplementary online material for details and a compilation of the coupling constants). Both the coupling between the subunits as well as the coupling of each subunit to its clean surface environment are considerably different. We present in figure 4(b) the total coupling constants for each subunit, which were obtained by summing the coupling constants of each subunit to all other (molecule-induced and clean surface) nearest-neighbor units.

The coupling constants listed in figure 4(b) give a direct measure of the energy scale for flipping the magnetic moment of the respective subunit with respect to all other subunits. The coupling constant evaluated from flipping the moment of a single Fe atom of the bare surface (unit 1 Fe-cs) is given as a reference[7]. Obviously, the energy scale to flip the moments of the molecule-induced hybrid magnetic subunits is larger than of a single surface Fe atom. This is a consequence of the fact that these hybrid subunits comprise three or four Fe surface atoms with enhanced exchange coupling in agreement with the results in [13, 17]. Most importantly, the

[7] According to the spin Hamiltonian used for evaluating the coupling constants this value is just half the energy difference between the FM state of the clean surface and the state with the single Fe moment flipped.

coupling constants of all molecule-induced hybrid magnetic subunits are considerably different as they vary by about 15%. This finally justifies that upon adsorption of TPT onto the 2 ML Fe/W(110) surface four distinguishable magnetic subunits below the molecular rings can be assigned, which are clearly distinct with respect to their magnetic exchange coupling behavior. The coupling values J_{unit} do not directly transform into switching fields for the magnetization reversal process since the switching will not take place by a direct flipping of the total moment of these different subunits. Stronger coupling counteracts thermal fluctuations and thus leads to an enhanced switching field as demonstrated by Monte-Carlo simulations [17, 19] and in experiments [11]. The clearly different coupling constants J_{unit} and our experimental SP-STM data both corroborate the formation of multiple distinguishable magnetic subunits within a single molecule–surface hybrid.

4. Conclusion

We found by both STM measurements and DFT calculations that the TPT molecule adsorbs in a chiral adsorption geometry on a 2 ML Fe/W(110) surface. This chirality expresses itself in an asymmetric geometry, in which all four aromatic rings of the molecule and the Fe atoms underneath are structurally and hence electronically different as indicated by both experimental as well as simulated STM topography images. Magnetically, an inversion of the spin polarization near the Fermi energy with respect to the Fe surface was found above the molecule in agreement with the general spin polarization inversion mechanism outlined for nonmagnetic organic molecules on magnetic surfaces [7]. The structural asymmetry was found to give rise to a variation of the spin polarization among the different phenyl rings showcasing an intramolecular modulation of the spin polarization on a nanometer length scale. The formation of multiple distinguishable magnetic subunits, each consisting of an aromatic ring and the Fe atoms directly underneath, is further confirmed by DFT calculations that reveal different magnetic moments and exchange coupling constants for the subunits as a consequence of their structural distinctiveness.

The perspective arising from our results is the generation of several magnetic subunits with different magnetic properties, in particular the exchange coupling, within a *single* adsorbed molecule. Organic chemistry can be used to design the linker groups between aromatic rings (each inducing a magnetic subunit upon adsorption) in order to tailor the mutual magnetic interactions between the subunits. Tuning parameters are for instance the length of the linker groups and their bonding character. Suitably adjusted magnetic couplings between the subunits are expected to lead to different switching thresholds under application of magnetic fields, spin currents, or other stimuli. This allows the generation of various intramolecular magnetic configurations with different (parallel and antiparallel) mutual magnetic alignment of the subunits. The coupling between them will allow for conditional switching of a given subunit depending on the magnetic alignment of the others. Hence, the threshold field of a given subunit depends on the magnetic state of the other subunits, ultimately enabling intramolecular spin-logic. The advantage of this organic chemistry route is the tunability of the magnetic interactions between *intramolecular* subunits, which is hardly achievable for the *intermolecular* interaction between randomly arranged hybrid magnets.

Acknowledgments

The computations were performed under the auspices of the VSR at the computer JUROPA and the GCS at the high-performance computer JUQUEEN operated by the JSC at the Forschungszentrum Jülich. We acknowledge financial support from the Volkswagen-Stiftung through the project 'Optically Controlled Spin Logic' [NA, VC, and DEB], from the Deutsche Forschungsgemeinschaft (DFG) through the Collaborative Research Center SFB 1238 (project C01), and from the European Commission under the ERC project 308051 'MOLSPINTRON' headed by Prof Paul Kögerler [VH].

References

[1] Sanvito S 2011 Molecular spintronics *Chem. Soc. Rev.* **40** 3336–55
[2] Dediu V, Murgia M, Matacotta F, Taliani C and Barbanera S 2002 Room temperature spin polarized injection in organic semiconductor *Solid State Commun.* **122** 181–4
[3] Scheybal A, Ramsvik T, Bertschinger R, Putero M, Nolting F and Jung T A 2005 Induced magnetic ordering in a molecular monolayer *Chem. Rev. Lett.* **411** 214–20
[4] Gambardella P *et al* 2009 Supramolecular control of the magnetic anisotropy in two-dimensional high-spin Fe arrays at a metal interface *Nat. Mater.* **8** 189–93
[5] Cinchetti M, Heimer K, Wüstenberg J P, Andreyev O, Bauer M, Lach S, Ziegler C, Gao Y and Aeschlimann M 2009 Determination of spin injection and transport in a ferromagnet/organic semiconductor heterojunction by two-photon photoemission *Nat. Mater.* **8** 115–9
[6] Javaid S *et al* 2010 Impact on interface spin polarization of molecular bonding to metallic surfaces *Phys. Rev. Lett.* **105** 077201

[7] Atodiresei N, Brede J, Lazic P, Caciuc V, Hoffmann G, Wiesendanger R and Blügel S 2010 Design of the local spin polarization at the organic-ferromagnetic interface *Phys. Rev. Lett.* **105** 066601
[8] Brede J, Atodiresei N, Kuck S, Lazić P, Caciuc V, Morikawa Y, Hoffmann G, Blügel S and Wiesendanger R 2010 Spin- and energy-dependent tunneling through a single molecule with intramolecular spatial resolution *Phys. Rev. Lett.* **105** 047204
[9] Kawahara S L, Lagoute J, Repain V, Chacon C, Girard Y, Rousset S, Smogunov A and Barreteau C 2012 Large magnetoresistance through a single molecule due to a spin-split hybridized orbital *Nano Lett.* **12** 4558–63
[10] Steil S, Großmann N, Laux M, Ruffing A, Steil D, Wiesenmayer M, Mathias S, Monti O L A, Cinchetti M and Aeschlimann M 2013 Spin-dependent trapping of electrons at spinterfaces *Nat. Phys.* **9** 242–7
[11] Raman K V *et al* 2013 Interface-engineered templates for molecular spin memory devices *Nature* **493** 509–13
[12] Caffrey N M, Ferriani P, Marocch S and Heinze S 2013 Atomic-scale inversion of spin polarization at an organic-antiferromagnetic interface *Phys. Rev.* B **88** 155403
[13] Brede J, Atodiresei N, Caciuc V, Bazarnik M, Al-Zubi A, Blügel S and Wiesendanger R 2014 Long-range magnetic coupling between nanoscale organic-metal hybrids mediated by a nanoskyrmion lattice *Nat. Nanotechnol.* **9** 1018–23
[14] Pang R, Shi X and Van Hove M A 2016 Manipulating magnetism at organic/ferromagnetic interfaces by molecule-induced surface reconstruction *J. Am. Chem. Soc.* **138** 4029–35
[15] Barraud C *et al* 2010 Unravelling the role of the interface for spin injection into organic semiconductors *Nat. Phys.* **6** 615–20
[16] Djeghloul F *et al* 2016 High spin polarization at ferromagnetic metal-organic interfaces: a generic property *J. Phys. Chem. Lett.* **7** 2310–5
[17] Callsen M, Caciuc V, Kiselev N, Atodiresei N and Blügel S 2013 Magnetic hardening induced by nonmagnetic organic molecules *Phys. Rev. Lett.* **111** 106805
[18] Khajetoorians A A, Wiebe J, Chilian B and Wiesendanger R 2011 Realizing all-spin-based logic operations atom by atom *Science* **332** 1062–4
[19] Friedrich R, Caciuc V, Kiselev N S, Atodiresei N and Blügel S 2015 Chemically functionalized magnetic exchange interactions of hybrid organic-ferromagnetic metal interfaces *Phys. Rev.* B **91** 115432
[20] Bode M, Krause S, Berbil-Bautista L, Heinze S and Wiesendanger R 2007 On the preparation and electronic properties of clean W(110) surfaces *Surf. Sci.* **601** 3308–14
[21] Hohenberg P and Kohn W 1964 Inhomogeneous electron gas *Phys. Rev.* **136** B864–71
[22] Kohn W and Sham L 1965 Self-consistent equations including exchange and correlation effects *Phys. Rev.* **140** 1133–8
[23] Kresse G and Hafner J 1994 *Ab initio* molecular-dynamics simulation of the liquid-metal-amorphous-semiconductor transition in germanium *Phys. Rev.* B **49** 14251–69
[24] Kresse G and Furthmüller J 1996 Efficient iterative schemes for *ab initio* total-energy calculations using a plane-wave basis set *Phys. Rev.* B **54** 11169–86
[25] Kresse G and Furthmüller J 1996 Efficiency of *ab-initio* total energy calculations for metals and semiconductors using a plane-wave basis set *Comput. Mater. Sci.* **6** 15–50
[26] Blöchl P E 1994 Projector augmented-wave method *Phys. Rev.* B **50** 17953–79
[27] Perdew J, Burke K and Ernzerhof M 1996 Generalized gradient approximation made simple *Phys. Rev. Lett.* **77** 3865–8
[28] Bethge H, Heuer D, Jensen C, Reshöft K and Köhler U 1995 Misfit-related effects in the epitaxial growth of iron on W(110) *Surf. Sci.* **331–333** 878–84
[29] Friedrich R, Caciuc V, Atodiresei N and Blügel S 2015 Molecular induced skyhook effect for magnetic interlayer softening *Phys. Rev.* B **92** 195407
[30] Barlow S M and Raval R 2003 Complex organic molecules at metal surfaces: bonding, organisation and chirality *Surf. Sci. Rep.* **50** 201–341
[31] Chen T, Wang D and Wan L J 2015 Two-dimensional chiral molecular assembly on solid surfaces: formation and regulation *Natl. Sci. Rev.* **2** 205–16
[32] Chiang S 1992 Molecular imaging by STM *Scanning Tunneling Microscopy I* (*Springer Series in Surface Science* vol 20) ed H-J Güntherodt and R Wiesendanger (Heidelberg: Springer)
[33] Lopinski G P, Moffatt D J, Wayner D D M and Wolkow R A 1998 Determination of the absolute chirality of individual adsorbed molecules using the scanning tunnelling microscope *Nature* **392** 909–11
[34] Mugarza A, Lorente N, Ordejón P, Krull C, Stepanow S, Bocquet M L, Fraxedas J, Ceballos G and Gambardella P 2010 Orbital specific chirality and homochiral self-assembly of achiral molecules induced by charge transfer and spontaneous symmetry breaking *Phys. Rev. Lett.* **105** 115702
[35] Baddeley C J and Richardson N V 2010 Chirality at metal surfaces *Scanning Tunneling Microscopy in Surface Science, Nanoscience and Catalysis* ed M Bowker and P R Davies (Weinheim: Wiley-VCH)
[36] Schlenhoff A, Krause S, Herzog G and Wiesendanger R 2010 Bulk Cr tips with full spatial magnetic sensitivity for spin-polarized scanning tunneling microscopy *Appl. Phys. Lett.* **97** 083104
[37] Atodiresei N, Caciuc V, Lazić P and Blügel S 2009 Chemical versus van der Waals interaction: the role of the heteroatom in the flat absorption of aromatic molecules C_6H_6, C_5NH_5, and $C_4N_2H_4$ on the Cu(110) surface *Phys. Rev. Lett.* **102** 136809
[38] Tersoff J and Hamann D R 1983 Theory and application for the scanning tunneling microscope *Phys. Rev. Lett.* **50** 1998–2001
[39] Wiesendanger R, Güntherodt H J, Güntherodt G, Gambino R and Ruf R 1990 Observation of vacuum tunneling of spin-polarized electrons with the scanning tunneling microscope *Phys. Rev. Lett.* **65** 247
[40] Perera U G E, Kulik H J, Iancu V, Dias da Silva L G G V, Ulloa S E, Marzari N and Hla S W 2010 Spatially extended Kondo state in magnetic molecules induced by interfacial charge transfer *Phys. Rev. Lett.* **105** 106601
[41] Wang W, Pang R, Kuang G, Shi X, Shang X, Liu P N and Lin N 2015 Intramolecularly resolved Kondo resonance of high-spin Fe(II)-porphyrin adsorbed on Au(111) *Phys. Rev.* B **91** 045440
[42] Friedrich R, Caciuc V, Atodiresei N and Blügel S 2016 Exchange interactions of magnetic surfaces below two-dimensional materials *Phys. Rev.* B **93** 220406
[43] Decker R, Brede J, Atodiresei N, Caciuc V, Blügel S and Wiesendanger R 2013 Atomic-scale magnetism of cobalt-intercalated graphene *Phys. Rev.* B **87** 041403